Food Hydrocolloids 159 (2025) 110681

Contents lists available at ScienceDirect

Food Hydrocolloids

journal homepage: www.elsevier.com/locate/foodhyd

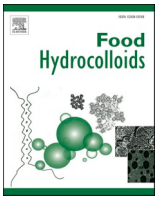

# Probing structural modification of milk proteins in the presence of pepsin and/or acid using small- and ultra-small-angle neutron scattering

Mengxiao Yang [a], Aiqian Ye [a,*], Zhi Yang [b], David W. Everett [a], Liliana de Campo [c], Harjinder Singh [a], Elliot Paul Gilbert [c,d]

[a] Riddet Institute, Massey University, Private Bag 11 222, Palmerston North, 4442, New Zealand
[b] Department of Human Nutrition, Food and Animal Sciences, University of Hawaii at Manoa, Honolulu, HI, 96822, USA
[c] Australian Centre for Neutron Scattering, Australian Nuclear Science and Technology Organization, New Illawarra Road, Lucas Heights, NSW, 2234, Australia
[d] Centre for Nutrition and Food Sciences, Queensland Alliance for Agriculture and Food Innovation, The University of Queensland, St. Lucia, Brisbane, QLD, 4072, Australia

ARTICLE INFO

*Keywords:*
Milk coagulation
Heat treatment
Pepsin
Protein
*In situ* digestion
Small- and ultra-small-angle neutron scattering (SANS and USANS)

ABSTRACT

Acid- and pepsin-induced milk protein coagulation plays a crucial role in the gastric digestion of milk. Real-time structural evolution at a nano- (e.g. colloidal calcium phosphate (CCP) and micelle) and micro- (gel network) level of unheated and heated (85 °C for 30 min) bovine milk was examined under acidic conditions and at low and high concentrations of pepsin using ultra-small- and small-angle neutron scattering (USANS and SANS), small-amplitude oscillatory rheometry and confocal scanning laser microscopy. Milk was treated with glucono-δ-lactone (GDL), pepsin or a combination of GDL and pepsin to induce coagulation. Heat-treated milk showed a faster increase in elastic storage modulus ($G'$) and scattering intensity (USANS and SANS) compared with unheated milk when coagulated with GDL or the combination of GDL and pepsin. At pH 6.3, heat treatment retarded pepsin (1.10 U/mL)-induced milk coagulation, with slower increases in $G'$ and scattering intensity. At a high concentration of pepsin (2000 U/mL) that mimics the concentration found in the stomach, general proteolysis followed coagulation. Heat treatment retarded coagulation but accelerated curd proteolysis. This study demonstrates how time-resolved USANS and SANS can be used to investigate the structural evolution of protein coagulation and degradation under gastric environment conditions at nano- and micro-metre length scales.

## 1. Introduction

In the gastric environment, the secretion of hydrochloric acid and pepsin and their combined action result in milk protein coagulation (Huppertz & Chia, 2021; Miranda & Pelissier, 1983; Ye, 2021). To better understand the coagulation behaviour of milk proteins during gastric digestion, considerable research has been conducted on pepsin-induced coagulation (Yang et al., 2022a; Yang et al., 2022b), acid-induced coagulation (Lucey, 2017) and coagulation induced by both pepsin and glucono-δ-lactone (GDL) (Roy, Ye, Moughan, & Singh, 2020) of casein micelles. At pH > 5, the specific hydrolysis of the $Phe^{105}$–$Met^{106}$ bond of κ-casein by pepsin yields the C-terminal glycosylated caseinomacro-peptide and para-κ-casein (Plowman & Creamer, 1995; Yang et al., 2022a). Casein micelles subsequently aggregate through hydrophobic association and electrostatic effects (Horne & Lucey, 2014) when a minimum amount of the caseinomacro-peptide has been hydrolysed (i.e. at a critical degree of hydrolysis). Acid-induced coagulation occurs when the isoelectric point (pH ~ 4.6) is approached, with GDL commonly used as an acidulant in model studies (Lucey, Teo, Munro, & Singh, 1997; Wang et al., 2019; Yang, Cheng, et al., 2023). In the presence of both GDL and pepsin, acidification and pepsin action occur simultaneously, resulting in different structural properties (Roy et al., 2020).

The high penetrating power and non-destructive nature of neutron radiation make small-angle neutron scattering (SANS) and ultra-small-angle neutron scattering (USANS) attractive techniques for the *in situ* structural analysis of protein gelation (Chodankar, Aswal, Kohlbrecher, Vavrin, & Wagh, 2009; Gilbert, 2019, 2023). These methods eliminate potential structural artefacts during extensive sample preparation required for electron microscopy. USANS has been used to study rennet- (Callaghan-Patrachar, Peyronel, Pink, Marangoni, & Adams, 2021) and plant protease- (tamarillin from Tamarillo fruits) (Li et al., 2018)

* Corresponding author.
*E-mail address:* a.m.ye@massey.ac.nz (A. Ye).

https://doi.org/10.1016/j.foodhyd.2024.110681
Received 21 July 2024; Received in revised form 9 September 2024; Accepted 24 September 2024
Available online 25 September 2024

induced bovine milk coagulation and GDL-induced skimmed bovine, sheep and goat milk coagulation (Wang et al., 2019; Yang, Cheng, et al., 2023). Micro-structural (fractal dimensional) evolutionary kinetics probed by USANS correlate well with the development of curd strength, as measured by the elastic shear modulus, $G'$ (Yang, Cheng, et al., 2023). SANS is a powerful technique for probing the internal structures of casein micelles and colloidal calcium phosphate (CCP) in casein micelles (de Kruif, 2014). Recently, SANS and USANS have been used to probe the structural modification of food proteins under *in vitro* digestion conditions. Pasquier et al. (2019) used SANS to probe structural changes in vegetable (cruciferin and napin) protein gels during *in vitro* gastric and intestinal digestion. Bayrak et al. (2021, 2023) investigated the structural changes in casein gels during simulated gastric digestion both with pepsin (2000 and 8000 U/mL) and without pepsin using SANS and USANS. The extensive $q$-range provided by combining SANS and USANS enables the monitoring of casein micelle structure evolution across various length scales both during coagulation and digestion. This covers a size range from protein-protein aggregation (~5 μm) to the CCP nanoclusters within the interior of the micelle (~5 nm).

Thermal processing is extensively used in the dairy industry to modify the textural properties and extend the shelf-life of milk products (Lewis, 1994). Under gastric conditions, with an associated decrease in pH and increase in pepsin concentration, heated (pasteurised and ultra-high-temperature treated) bovine milk forms curd with fragmented and crumbly structures and unheated milk forms more cohesive curd (Ye, Cui, Dalgleish, & Singh, 2017; Ye et al., 2019). As a result, faster rates of protein hydrolysis and fat globule release have been observed during the gastric digestion of heated bovine whole milk. The effects of heat treatment on the rheological properties and micro-structural characteristics are significantly different between rennet-induced coagulation, acid-induced coagulation and combination-induced coagulation gels (Anema, Lee, & Klostermeyer, 2007, 2011; Lucey, Tamehana, Singh, & Munro, 2001; Lucey, Wilbanks, & Horne, 2022; Yang, Ye, et al., 2023).

In this study, acid (GDL)-induced coagulation (AC), pepsin-induced coagulation (PC) and coagulation induced by a combination of both GDL and pepsin (CC) in unheated and heated milk were examined. Moreover, to investigate the changes during the degradation of casein curd induced by pepsin, GDL and a high pepsin concentration were added to unheated and heated milk. Time-resolved SANS and USANS were used to probe milk protein structural evolution at length scales from a few nanometres to several micrometres. The structural parameters obtained from these scattering studies (e.g. fractal dimensions and aggregate size), combined with rheological characterisation and confocal laser scanning microscopy, shed light on the protein structural evolution of unheated and heated bovine milk during coagulation and proteolysis during gastric digestion.

## 2. Materials and methods

### 2.1. Materials

Raw bulk whole bovine milk was collected from Massey University No. 4 Dairy Farm (Palmerston North, New Zealand) in March 2022. Upon receipt of the milk samples, 0.02% (wt/wt) sodium azide (Merck KGaA, Darmstadt, Germany) was added to prevent microbial growth. The cream layer was carefully removed by centrifugation of raw whole milk at 3000×$g$, 15 min, 4 °C (Heraeus X3R; Thermo Fisher Scientific, Inc., USA). The skimmed cow milk was then freeze-dried. Porcine pepsin (EC 3.4.23.1; Sigma-Aldrich, St. Louis, MO, USA) with stated activity of 541 U/mg protein was dissolved in Milli-Q water (5 mg per 5 mL; activity 541 U/mL). All other chemicals (analytical grade) were obtained from Sigma-Aldrich unless otherwise specified.

### 2.2. Milk preparation characterisation

Skimmed milk powders were reconstituted in 100% $H_2O$ or 100% $D_2O$ at 3 wt% protein content by gentle magnetic stirring overnight to allow protein hydration. The samples were stored at 4 °C for up to 5 days and equilibrated to 37 °C before further use. Reconstituted bovine milk contained 2.97% protein (2.37% casein), 0.15% fat and 3.78% lactose, as determined using a Milkoscan (Foss, Hilleroed, Denmark). A portion of the reconstituted milk was heated at 85 °C for 30 min in a water bath.

### 2.3. Sample preparation

The preparation of each sample is shown in Table 1. Samples arising from acid-induced coagulation (AC), pepsin-induced coagulation (PC), coagulation induced by a combination of pepsin and acid (CC) and high pepsin concentration (HP) of unheated milk are denoted as ACU, PCU, CCU and HPU, respectively, and those for heated milk as ACH, PCH, CCH and HPH, respectively. Associated $D_2O$-dispersed samples, namely, ACU-$D_2O$, PCU-$D_2O$ and CCU-$D_2O$, were prepared to enable specific CCP features to be highlighted from the SANS measurements.

GDL powder (2 wt%, under which the pH of the milk system decreased from 6.7 to ~4.3 over 2 h and to ~3.8 over 8 h) was added to milk with magnetic stirring at 25 °C for 1 min before transferring to the rheometer or USANS/SANS sample cells. Pepsin solutions were added to the samples at a ratio of 10 μL per 1 mL of milk, resulting in final pepsin concentrations of 1.10 and 0.24 U/mL for PC and CC, respectively. The pepsin concentration was selected on the basis of the preliminary rheological experiments: for each pepsin concentration, significant increases in the storage modulus ($G'$) of CC occurred at pH above 4.6 and significant increases in the $G'$ of PC occurred within 60 min and reached equilibrium after approximately 2 h. For HP samples, the milk was mixed with GDL (2 wt%) and pre-loaded into the rheometer or into the SANS/USANS sample cells, followed by the addition of the pepsin solution [2000 U/mL, mimicking gastric conditions (Brodkorb et al., 2019)] and mixed well.

During the coagulation reaction, the pH value of each sample was determined *in situ* by dipping a HALO Bluetooth wireless pH electrode (HI11102, Hanna instruments, Smithfield, RI, USA) into the milk samples incubated in a water bath set at 37 °C at the required time (the pH was recorded every minute for 2 h for AC, PC and CC and 8 h for HP).

### 2.4. Rheological measurements

Rheological measurements were conducted in an AR-G2 magnetic-bearing rheometer (TA Instruments, Crawley, West Sussex, UK) with standard Peltier concentric cylinder geometries (a cup and a rotor with radii of 15 and 14 mm, respectively). Low-viscosity silicone oil was added at the top of the geometries to avoid evaporative loss during measurements. A time-sweep measurement was performed at a constant strain of 1% and a constant frequency of 1 Hz to monitor the rheological properties over time (2 h for AC, PC and CC; 8 h for HP). The storage modulus ($G'$) and the viscous modulus ($G''$) were recorded every minute

**Table 1**
Preparation of acid-induced coagulation (AC), pepsin-induced coagulation (PC), combination coagulation (CC) and high pepsin concentration (HP) samples.

| Sample | Initial pH | GDL (wt/wt) | Pepsin (U/mL sample) |
|---|---|---|---|
| AC | 6.7 | 2% | – |
| PC | 6.3[a] | – | 1.10 |
| CC | 6.7 | 2% | 0.24 |
| HP | 6.7 | 2% | 2000 |

[a] Note: The pH of the PC sample was pre-adjusted to 6.3 by the slow addition of 1 M HCl, because pepsin-induced hydrolysis of κ-casein occurs most effectively at pH 6.3 (Yang et al., 2022). The same treatment was performed on unheated milk and heated milk.

at 37 °C.

### 2.5. USANS

Sample preparation for USANS measurements is described in Section 2.3. The prepared samples (~1.5 mL) were carefully transferred into demountable USANS sample cells (thickness of 1 mm) using a disposable syringe and placed on the KOOKABURRA instrument at the OPAL facility at the Australian Nuclear Science & Technology Organisation (ANSTO), Sydney, Australia (Rehm, Brûlé, Freund, & Kennedy, 2013; Rehm et al., 2018). All measurements were performed at 37 °C under tumbling using a neutron wavelength, λ, of 4.74 Å with a 29 mm Gd aperture. Milk before coagulation was measured by USANS over an extended $q$ range of ~$3.5 \times 10^{-5}$–0.01 $Å^{-1}$, corresponding to a length scale from approximately 60 to 18 μm (Yang et al., 2022c).

The untreated samples (unheated milk and heated milk) were fitted with the Guinier–Porod model in SasView software (version 5.0.5, https://www.sasview.org/) which describes the radius of gyration and the power law behaviour of a scattering system (Hammouda, 2010). This relationship is given by the following:

$$\mathrm{I}(q) = \frac{\mathrm{G}}{q^{s}} \exp\left[\frac{-\mathrm{q}^{2} Rg^{2}}{3 - \mathrm{S}}\right], q \le q_{1},$$

$$I(q) = \frac{D}{q^{m}}, q \ge q_{1}, \quad \text{(Equation 1)}$$

where $q$ is the magnitude of the scattering vector, $I(q)$ is the scattered intensity, $R_g$ is the radius of gyration, m is the Porod exponent and $G$ and $D$ are the Guinier and Porod scale factors, respectively. S is equal to zero for spheres in this study. The Guinier form is used for $q \le q_1$, and the Porod form is used for $q \ge q_1$. Enforcing the continuity of the Guinier and Porod functions and their derivatives yields the following:

$$q_{1} = \frac{1}{R_{g}} \sqrt{\frac{3\mathrm{m}}{2}},$$

$$D = G \exp\left(\frac{-{q_1}^{2} Rg^{2}}{3}\right) {q_1}^{m} = G \exp\left(-\frac{m}{2}\right)\left(-\frac{3m}{2}\right)^{\frac{m}{2}} \frac{1}{Rg^{m}}.$$

(Equation 2)

For time-resolved USANS data, it should be noted that, similar to other Bonse–Hart-type instruments, KOOKABURRA uses an analyser crystal that must change position to collect data for each $q$ value representing a point-by-point measurement. Consequently, careful consideration is required for optimal data acquisition for systems that change with time. Data collection over an extended $q$ range over a short time interval is not possible; one full scan with acceptable statistics takes more than 30 min. To reduce the measuring time during the reaction therefore the analyser crystal angle was deliberately fixed and a single $q$ value ($1 \times 10^{-4}$ $Å^{-1}$) was applied to monitor the absolute intensity change (corresponding to a length scale of approximately 6 μm).

### 2.6. SANS

SANS measurements were performed on the QUOKKA instrument at ANSTO, Sydney, Australia (Wood et al., 2018). The samples were prepared under the same conditions as those for USANS, and ~350 μL of the mixed samples was loaded into the banjo-type cells and measured at 37 °C. Time-resolved SANS data were collected using a focussing optics configuration with λ of 8.1 Å with 10% resolution, equal source-to-sample distance (SSD) and sample-to-detector distance (SDD) of 20 m, a source aperture diameter of 30 mm and sample aperture diameter of 12.5 mm. In addition, full $q$ range data on QUOKKA were collected for the following instrument configurations: (i) SSD = SDD = 20 m, (ii) SSD = SDD = 8 m and (iii) SSD = 4 m and SDD = 1.3 m, the latter with 300 mm detector offset, using a λ of 5 Å with 10% resolution. These configurations used a source aperture diameter of 50 mm and sample aperture diameter of 12.5 mm. The data collected cover a total $q$ range from ~0.0007 to 0.01 $Å^{-1}$. SANS data were reduced following a standard procedure (Kline, 2006) using the Igor Pro software (Wavemetrics, USA) with the scattering from an empty cuvette subtracted as a background. Data for the $D_2O$-only dispersed milk sample (4 wt% protein content) was collected on the BILBY instrument at OPAL (Sokolova et al., 2019) in a previous study by Yang, Cheng, et al. (2023). The intensity of the untreated samples (unheated milk and heated milk) in SANS were fitted to a Guinier–Porod model. The data at 0.0007 $Å^{-1} < q < 0.0022$ $Å^{-1}$ during the reaction at 0, 5, 10, 15, 20, 30, 60, 90 and 120 min for each sample (and two more time point at 240, 480 min for HPU, HPH) were fitted to a power law model given as follows:

$$I(q) = scale \times q^{m}, \quad \text{(Equation 3)}$$

where $m$ is the power law exponent, from which the nature and geometry of the scattering object can be described.

To explore the differences in CCP between AC, PC and CC samples, GDL or/and pepsin were added to the milk reconstituted in $D_2O$ (same conditions as those for the $H_2O$-dissolved samples) to enhance the scattering contrast. The resulting mixture was then injected into a SANS banjo cell and incubated in an oven at 37 °C for 2 h (regarded as equilibrated samples). The equilibrated samples were subsequently probed using QUOKKA under the same conditions as those for the $H_2O$-dissolved samples.

### 2.7. Confocal laser scanning microscopy

Coagulum micro-structures were observed using confocal laser scanning microscopy. Fast Green fluorescent dye (3 μL; 1% wt/vol) was added to skimmed milk (100 μL) and mixed for 30 s. After pre-warming to 37 °C, the mixture was then transferred to the cavity of a glass microscope slide, covered with a glass coverslip and incubated for 2 h at 37 °C. The edges of the cover slip were sealed with nail polish to prevent evaporation. Each sample was examined using a Leica TCS SP5 confocal laser scanning microscope (Leica Micro-systems) with a 63 × magnification lens.

### 2.8. Statistical analysis

Samples were prepared in triplicate for the measurements of pH and rheology; values are expressed as mean ± standard deviation. Experimental data were analysed by running analysis of variance (ANOVA) tests using Prism 8 (GraphPad Software Inc., San Diego, CA, USA). Differences were considered significant at $P < 0.05$.

## 3. Results and discussion

### 3.1. USANS probing of unheated and heated milk

The USANS profiles (which are slit-smeared using the Bonse-Hart optics) over an extended $q$ range ($3.5 \times 10^{-5}$ $Å^{-1} < q < 10^{-2}$ $Å^{-1}$) for the unheated- and heated-milk samples are shown in Fig. 1; the desmeared data are shown in Fig. S1. In the high-$q$ region, a Guinier shoulder feature (building block size, R) can be observed at $q$ between 0.002 and 0.004 $Å^{-1}$ (arrow), indicating scattering from individual casein micelles (unheated milk) or casein micelle–whey protein complexes (heated milk) (Li et al., 2018; Wang et al., 2019). In the limit of low q, there is an upturn in the scattering from particles of the order of greater than 20 μm; this may arise from residual fat globules in the skim milk. A Guinier–Porod model was applied over a limited $q$ range excluding this upturn to yield values for $R_g$ associated with casein micelle dimensions. A slightly larger casein micelle size was found in the heated samples ($R_g$ = 51.2 nm) than in the unheated sample ($R_g$ = 60.5 nm) giving corresponding particle diameters [$2 \times R$, $R = (5/3\ R_g^2)^{0.5}$] of

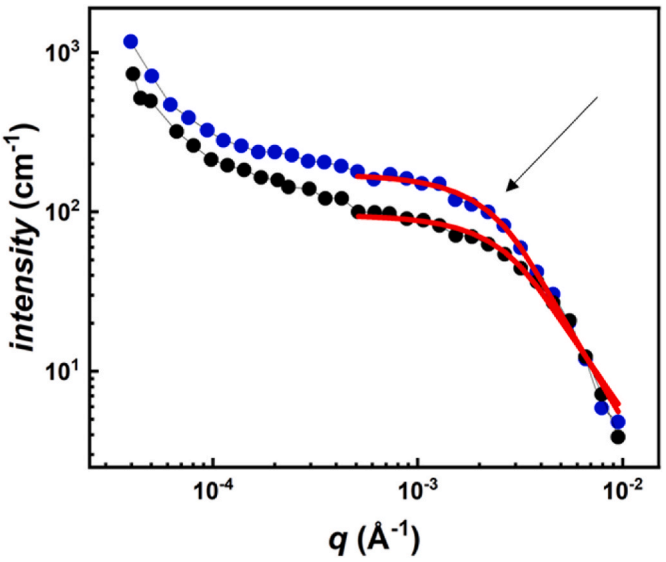


**Fig. 1.** Reduced (slit-smeared) USANS of unheated (●) and heated bovine skimmed milk (●). The curves at $5 \times 10^{-4}$ Å$^{-1}$ < $q$ < $10^{-2}$ Å$^{-1}$ were fitted with a Guinier–Porod model (red curves). Arrow points to a Guinier shoulder feature (see Section 3.1).

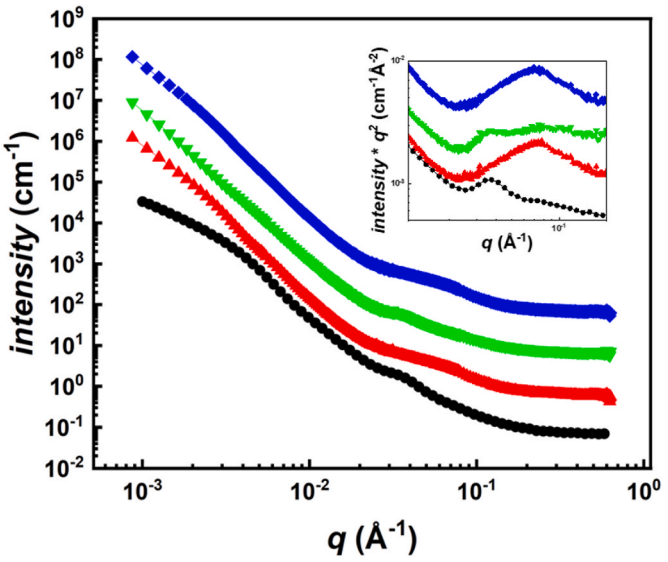


**Fig. 2.** (A) SANS patterns of D2O-dissolved milk samples coagulated by GDL ('ACU-D2O') (■), pepsin ('PCU-D2O') (▼), their combination ('CCU-D2O') (▲), as well as D2O-only dispersed milk sample (●); data shown following high $q$ background subtraction. Data have been offset for clarity (ACU by factor of 10, PCU by factor of 100, and CCU by factor of 1000). Inset shows the corresponding Kratky plots highlighting the structure of CCP nano-clusters; data have been offset for clarity (ACU by factor of 4, PCU by factor of 8, and CCU by factor of 16).

132 ± 4 and 156 ± 3 nm for unheated and heated milk, respectively; the Guinier-type feature of unheated and heated milk can also be observed in the SANS results. These values agree well with those from previous SANS/USANS studies on casein micelles from bovine milk (Day, Raynes, Leis, Liu, & Williams, 2017; de Kruif, 2014; Liu et al., 2017).

### 3.2. Probing calcium phosphate nano-cluster features

It has been reported that the calcium phosphate nano-cluster (CCP) feature was only observable in samples reconstituted in $D_2O$ by SANS [despite variations in curd firmness or brittleness between milk samples prepared in $D_2O$ and $H_2O$ (Bayrak et al., 2021)]. In fact, it is rather more the case that the CCP structure factor peak at approximately 0.035 Å$^{-1}$ is most prominent when the solvent is contrast-matched to protein (approximately 41% $D_2O$) and is masked in $H_2O$ (de Kruif, 2014). To enable CCP peak observation, SANS patterns for the full $q$ range from equilibrated samples in $D_2O$ were collected, namely ACU-$D_2O$, PCU-$D_2O$ and CCU-$D_2O$ and are shown in Fig. 2 (corresponding Kratky plots for the same data highlighting the structure of CCP nano-clusters are shown as inset). According to previous studies, the appearance of a shoulder at approximately 0.035 Å$^{-1}$ is attributed to the interference between calcium phosphate nano-clusters (CCP) within the casein micelle (de Kruif, 2014; Yang, Cheng, et al., 2023) such that the peak position is related to the average correlation distance between neighbouring CCP particles. After coagulation, the peak position in PCU-$D_2O$ remained at $q \approx 0.035$ Å$^{-1}$, whereas the peak positions in ACU-$D_2O$ and CCU-$D_2O$ shifted to a higher $q$ at ≈ 0.070 Å$^{-1}$.

Native casein micelles (at fresh bovine milk pH of ~6.7) are stabilised by negative charges and steric repulsion. When the pH is below 5.0, the CCP nano-clusters within casein micelles gradually dissolved (Lucey, 2017). According to Yang, Cheng, et al. (2023), the acidity (pD-value) of milk was close to 4.0 after a 2-h reaction time with the addition of GDL powder (2.5 wt%). Under these conditions (pD < 4), the CCP nano-clusters within casein micelles undergo complete dissolution in ACU-$D_2O$ and CCU-$D_2O$ samples. This is consistent with the SANS observations. Although the CCP correlations in PCU-$D_2O$ did not change after the 2-h reaction time, for ACU-$D_2O$ and CCU-$D_2O$, the shift to higher $q$ (shorter distance) is not a consequence of more efficient CCP packing but rather the packing of smaller scattering particles or nano-pores left by the dissolution of the CCP (Singh, Hemar, Gilbert, Wu, & Yang, 2020); the acidification of milk induces the progressive fading of the CCP feature due to the acid-induced dissociation of CCP in ACU-$D_2O$ and CCU-$D_2O$ samples, leading to the small protein inhomogeneities and/or structural arrangements (Moitzi, Menzel, Schurtenberger, & Stradner, 2011), whereas at constant pD, for the CCP region in PCU-$D_2O$, casein micelles remained intact in the milk curd (Li et al., 2018; Schaefer, Martin, Wiltzius, & Cannell, 1984). The CCP in heated milk was not determined in this study as previous studies have suggested that heat treatment does not alter the dissolution kinetics of CCP in bovine milk (Singh, 1995; Yang, Cheng, et al., 2023).

### 3.3. Acid-induced milk coagulation and the effect of preheat treatment

With an addition of 2% GDL, the pH of ACU and ACH decreased from 6.7 to ~4.3 after the 2-h reaction time (Fig. 3A). The changes in the storage modulus ($G'$) of ACU and ACH with time are shown in Fig. 3B: the $G'$ of both samples showed a lag phase in the early stages, and after the onset of coagulation, $G'$ increased significantly, indicating an enhancement in curd firmness. The coagulation properties, including the coagulation time ($t_1$, the first time point when $G'$ significantly increases), firming rate ($dG'/dt$) and maximum $G'$ ($G'_{max}$), are summarised in Table 2. ACU coagulated at ~40.5 min when the pH was ~4.90, near the isoelectric point of the casein proteins. ACH had shorter coagulation times (~34.8 min) and higher pH values (~5.07) at the coagulation point. Within 2 h of reaction, the firming rate and $G'_{max}$ of ACH were higher than those of ACU. In agreement with Lucey, Tamehana, Singh, and Munro (1998), because of the association of denatured whey proteins with casein micelles during heat treatment, a shorter coagulation time and higher firming rate, $G'_{max}$ and pH at coagulation point were observed in the heated-milk sample.

At $q = 1 \times 10^{-4}$ Å$^{-1}$ (corresponding to length scales on the order of μm), the changes in the USANS absolute scattering intensity as a function of time for ACU and ACH are shown in Fig. 3C. The changes in the absolute intensity in the USANS were observed from the beginning, which were related to the increases in the particle size or volume fraction of the aggregates. Note that the rapid increase in intensity justified

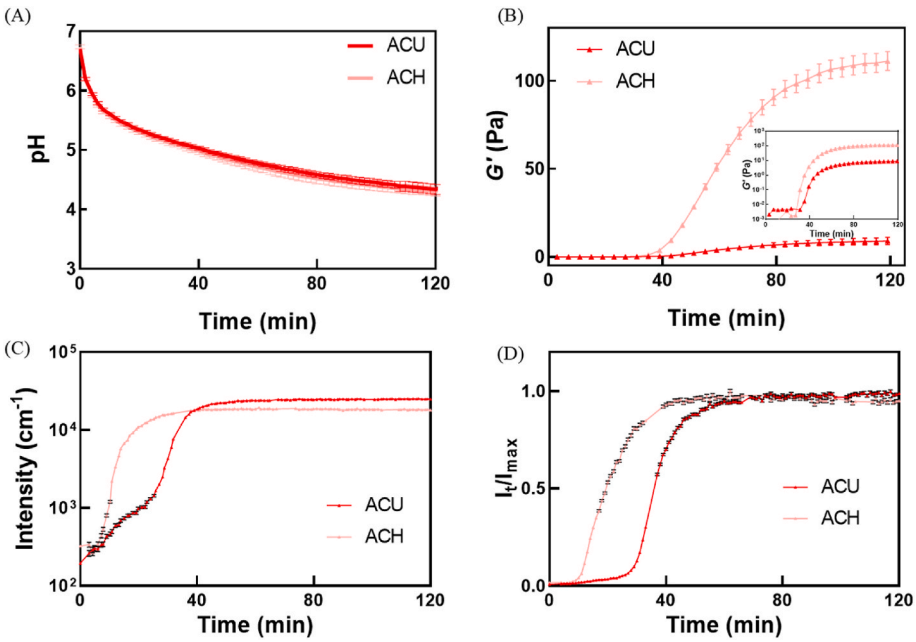


**Fig. 3.** Evolution of pH (A), $G'$ (B) (inset shows $G'$ on a logarithmic scale), absolute USANS intensity at $q = 1 \times 10^{-4}$ Å$^{-1}$ (C), normalised USANS intnsities ($I_t/I_{max}$, $I_t$ is the absolute USANS intensity at $q = 1 \times 10^{-4}$ Å$^{-1}$, $I_{max}$ is the maximum intensity during the reaction time) (D), for unheated milk (ACU) and heated milk (ACH).

**Table 2**
Coagulation properties of milk in different samples.

| | ACU | ACH | PCU | PCH | CCU | CCH | HPU | HPH |
|---|---|---|---|---|---|---|---|---|
| $t_1$ (min) | 40.5 ± 2.4$^{A}$ | 34.8 ± 1.6$^{A}$ | 20.6 ± 0.1$^{B}$ | 21.7 ± 6.9$^{B}$ | 25.6 ± 1.6$^{B}$ | 12.8 ± 1.2$^{C}$ | 2$^{D}$ | 2$^{D}$ |
| $t_2$ (min) | 122 [a] | 122 [a] | 122 [a] | 122 [a] | 37.2 ± 2.0 | 25.5 ± 2.0 | 13.8 ± 1.6 | 4.2 ± 2.1 |
| $t_3$ (min) | – | – | – | – | 47.8 ± 2.0 | 40.7 ± 2.0 | 86.4 ± 5.5 [c] | 49.8 ± 2.1[c] |
| $pH_1$ | 4.90 ± 0.05 | 5.07 ± 0.05 | 6.30 ± 0.01 | 6.30 ± 0.01 | 5.26 ± 0.01 | 5.62 ± 0.15 | – | – |
| $pH_2$ | 4.34 ± 0.09[b] | 4.30 ± 0.08[b] | 6.30 ± 0.01[b] | 6.30 ± 0.01[b] | 5.08 ± 0.03 | 5.18 ± 0.08 | 5.34 ± 0.01 | 6.06 ± 0.19 |
| $pH_3$ | – | – | – | – | 4.97 ± 0.03 | 4.80 ± 0.08 | – | – |
| $FR_1$ (Pa/min) | 0.21 ± 0.02 | 2.83 ± 0.14 | 1.42 ± 0.01 | 0.34 ± 0.02 | 0.29 ± 0.09 | 2.48 ± 0.87 | – | – |
| $FR_2$ (Pa/min) | – | – | – | – | −0.13 ± 0.08[d] | −0.83 ± 0.02[d] | −1.44 ± 0.38[d] | −3.14 ± 0.75[d] |
| $FR_3$ (Pa/min) | – | – | – | – | 0.43 ± 0.10 | 0.81 ± 0.01 | – | – |
| $G'_{max1}$ (Pa) | 8.98 ± 0.21$^{C}$ | 111.29 ± 2.83$^{A}$ | 37.61 ± 1.42$^{B}$ | 22.24 ± 0.34$^{C}$ | 2.72 ± 1.04$^{C}$ | 18.01 ± 6.36$^{B}$ | 37.8 ± 10.0$^{B}$ | 20.9 ± 16.7$^{C}$ |
| $G'_{max2}$ (Pa) | – | – | – | – | 18.04 ± 2.66 | 42.16 ± 4.14 | – | – |

The acid-induced coagulation (AC), pepsin-induced coagulation (PC), combination coagulation (CC) and high pepsin concentration (HP) samples for unheated milk are denoted ACU, PCU, CCU and HPU. The respective heated milk samples are denoted ACH, PCH, CCH and HPH.
The time point in this table takes into account the time required for sample preparation, i.e. 2 min from the moment the sample was mixed until the first time point recorded using a rheometer. $t_1$ refers to the first time point when $G'$ significantly increases, regarded as coagulation time. $t_2$ refers to the first time point when $G'$ significantly decreases. $t_3$ refers to the second time point when $G'$ significantly increases.
$pH_1$, $pH_2$ and $pH_3$ refer to the pH values at times $t_1$, $t_2$ and $t_3$, respectively.
The maximum absolute slope of the $G'$ curve ($dG'/dt$) is defined as the firming rate (FR). $FR_1$ refers to the firming rate from $t_1$ to $t_2$. $FR_2$ refers to the firming rate from $t_2$ to $t_3$. $FR_3$ refers to the firming rate from $t_3$ to the end time point.
$G'_{max1}$ refers to the maximum storage modulus between $t_1$ and $t_2$. $G'_{max2}$ refers to the maximum storage modulus from $t_3$ to the end time point.
[A–D] Mean values between samples in the same column with different superscripts are significantly different ($P < 0.05$). The results are expressed as the mean ± the standard deviation of the mean (n = 3).
[a] The end time point during measurement.
[b] The pH at end time points during measurement.
[c] The time point when $G'$ stops decreasing.
[d] Negative values correspond to a decreasing rate of curd firmness.

the approach used for collecting USANS data, where a fixed $q$ value was selected for monitoring. At the coagulation time ($t_1$), the absolute scattering intensities were ~18,000 and ~17,000 cm$^{-1}$ for ACU and ACH, respectively. To better examine these changes, the evolution of normalised intensities ($I_t/I_{max}$, $I_t$ is the absolute USANS intensity at $q = 1 \times 10^{-4}$ Å$^{-1}$, $I_{max}$ is the maximum intensity during the reaction time) as a function of reaction time is shown in Fig. 3D. The $I_t/I_{max}$ of the AC samples showed a lag phase, log phase and stationary phase. The significant increase (log phase) in ACH (~10 min, pH 5.55) occurred more rapidly than that in ACU (~30 min, pH 5.06), with a similar increase in rate (slope) during the log phase. In addition, the $I_t/I_{max}$ of ACH reached a plateau (stationary phase) at ~35 min, which was faster than that of ACU at ~50 min. These results suggest that heat treatment markedly accelerates the growth of the aggregates. Although the rheological results (Fig. 3B) showed that coagulation did not occur at the beginning, the scattering results (Fig. 3C) indicated that the size of the aggregates increased from the beginning. However, the rate of increase in aggregate size was very slow, leading to a noticeable lag phase in the normalised intensity (Fig. 3D). This is supported by molecular weight measurements using light scattering (Dalgleish, Brinkhuis, & Payens, 1981). After the

addition of rennet, an initial lag phase with no increase was observed, followed by a short intermediate phase, before the molecular weight became linearly proportional to time (Dalgleish et al., 1981).

Time-resolved SANS profiles of ACU and ACH are shown in Fig. 4A and **B**, respectively. In general, the SANS scattering patterns of ACU and ACH during coagulation are similar. As time progressed, the intensity increased in the lower $q$ range ($q < 0.003$ Å$^{-1}$) and decreased at higher $q$. A Guinier feature could be observed until approximately 20 min (describing the size of the aggregates), but this feature disappeared after approximately 20 min, which might reflect an increase in aggregate size, i.e. shift to lower $q$, and presumably could be observed using USANS. Consequently, Guinier model fitting was not used in this study. Instead, a power law model was used to fit the curves obtained at different time points (5, 10, 15, 20, 30, 60, 90 and 120 min) within 0.0007 Å$^{-1}$ < $q$ < 0.0022 Å$^{-1}$. The parameters obtained from the fits are listed in Table S1. The changes in the power law exponent ($m$) with time are shown in Fig. 4C. The obtained power law exponents from the SANS results showed an increase over time. The nature and geometry of the scattering object can be determined through the power law exponent (m). Values of 0 < m < 3 may refer to mass fractal structures (three-dimensional self-similarity over large-scale lengths), which indicates the compactness of the object (Martin & Hurd, 1987). For mass fractals, a higher power law exponent indicates a more compact structure (Yu et al., 2019). A higher power law exponent ($m$) was obtained from ACH compared with ACU at each time point within the initial 20-min period, indicating a more extensive aggregate structure in ACH than in ACU. A power law between 3 and 4 is usually interpreted as arising from surface geometry, with a smooth surface giving a value of 4 and values approaching 3 indicating increasing roughness (Mata, Udabage, & Gilbert, 2011). At 30 min, the lower $m$ ~3 of ACH indicates a relatively rough surface compared with ACU (which has $m$ ~4).

Confocal laser scanning microscopy (CLSM) images of ACU and ACH at 2 h are shown in Fig. 4D. The protein stained by Fast Green appeared as green, and the serum voids were shown in black. The structure of ACU exhibited a looser protein network structure with greater porosity than that of ACH. Similar observations were found in previous microscopic studies of acid gels induced by GDL (Wang et al., 2019; Yang, Cheng, et al., 2023).

Heat treatment of milk at pH 6.7 and 85 °C for 30 min resulted in denaturation of more than 80% of whey proteins, and approximately 70% of them were associated with casein micelles involving κ-casein (Oldfield, Singh, Taylor, & Pearce, 2000). The associated whey proteins could be a reason for the higher surface roughness, resulting in a lower $m$ ~3 for ACH compared with ACU. Denatured whey proteins associated with casein micelles become susceptible to aggregation during acidification and facilitate the cross-linking of casein particles in curd networks. This leads to an increase in the number and strength of bonds between protein particles, resulting in the higher $G'_{max}$ observed in ACH than in ACU. In addition, the isoelectric pH values of the whey proteins are ~4.8–5.2, which are higher than those of the casein proteins (De Wit, 1981). It is therefore likely that enhanced protein–protein interactions occur between denatured whey proteins near the isoelectric pH values because of the heat-induced exposure of the previously buried hydrophobic groups (Zhu & Damodaran, 1994). Therefore, it takes less time for the increases in $G'$ and USANS intensity in sample ACH compared with ACU.

### 3.4. Pepsin-induced milk coagulation and the effect of preheat treatment

No pH changes were observed during coagulation after the addition of pepsin only, and the pH of both unheated and heated samples remained constant at ~6.3 (Fig. 5A). As shown in Fig. 5B, $G'$ showed a lag phase and significant increases in $G'$ of PCU and PCH were observed at ~20.6 and 21.7 min, respectively. The $G'$ of PCU reached a plateau value (~40 Pa) at ~70 min. The $G'$ of PCH continually increased with reaction time over 2 h but was lower than that of PCU at 120 min (Fig. 5B). The increases in $G'$ were due to the hydrolysis of κ-casein and the aggregation of the para-casein micelles by hydrophobic association (Yang et al., 2022a). The evolution of $G'$ is in accordance with a previous study on pepsin-induced milk coagulation that reported a slower firming

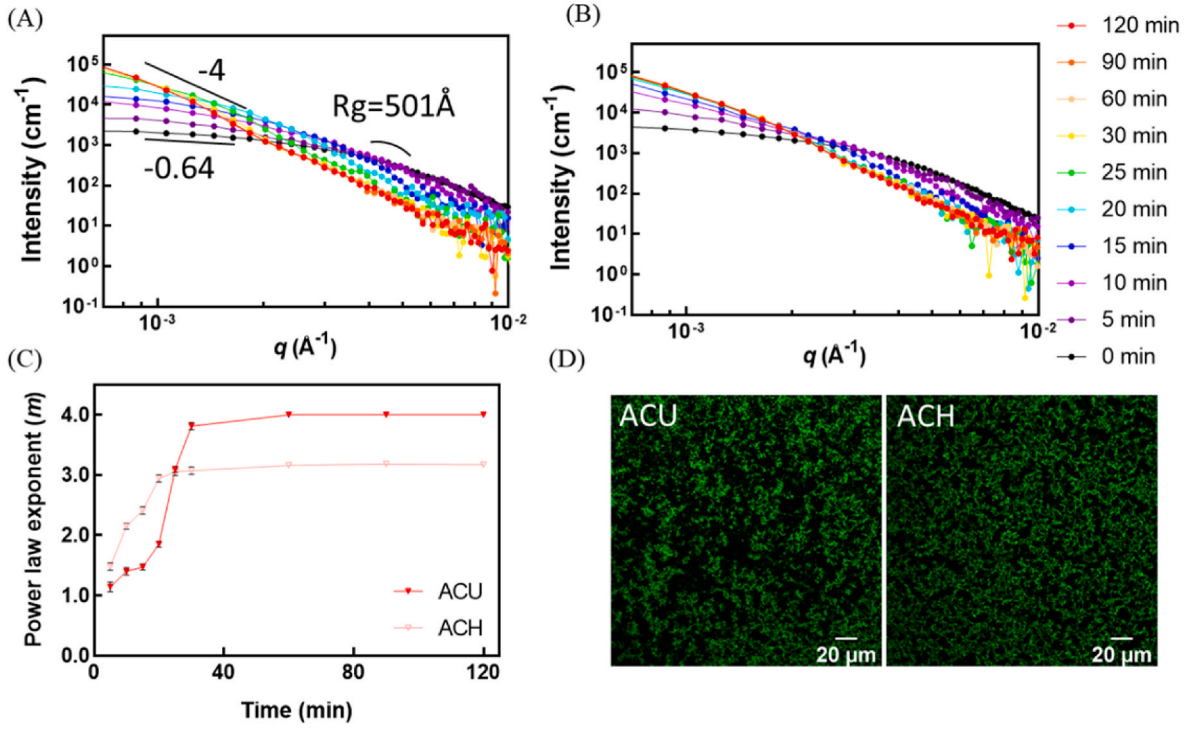


**Fig. 4.** Evolution of time-resolved SANS intensity data at 0.0007 Å$^{-1}$ < $q$ < 0.01 Å$^{-1}$ of (A) ACU and (B) ACH. (C) Power law exponent ($m$) obtained from the power law fitting of SANS associated with (A) and (B). (D) Confocal laser scanning micro-graphs of ACU and ACH at 2 h. The stained protein networks are in green. The scale bars are 20 μm for both micro-graphs.

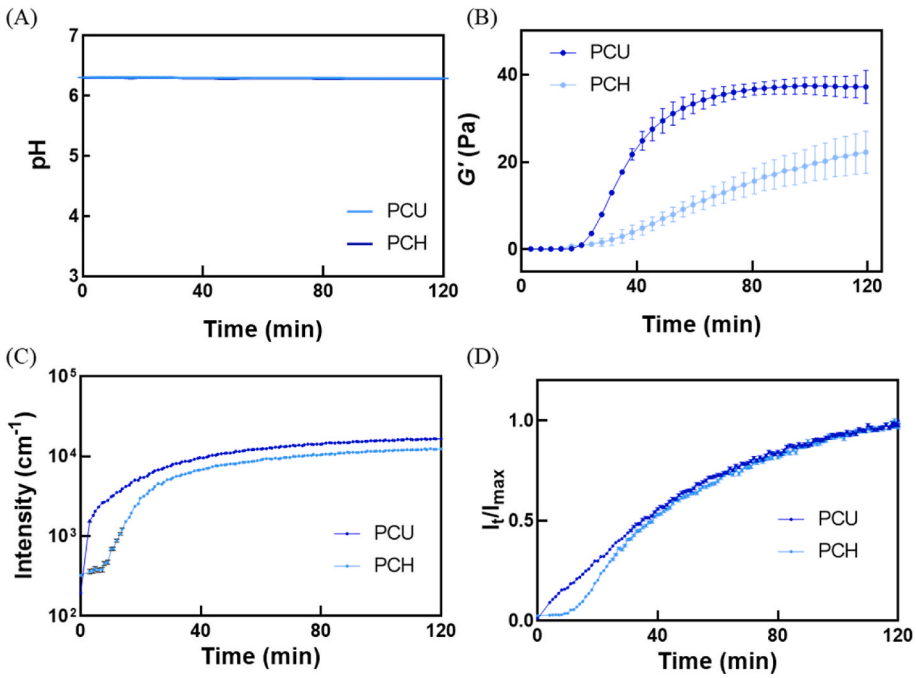


**Fig. 5.** Evolution of pH (A), $G'$ (B), absolute USANS intensity at $q = 1 \times 10^{-4}$ Å$^{-1}$ (C), normalised USANS intensities ($I_t/I_{max}$) (D) for unheated milk (PCU) and heated milk (PCH).

rate for a heated-milk sample (Yang et al., 2022b).

An immediate increase in absolute USANS intensity for PCU was observed once pepsin was added, and a lag phase of intensity was observed for PCH (Fig. 5C). At the coagulation time ($t_1$), the absolute scattering intensities were ~5000 and ~3000 cm$^{-1}$ for PCU and PCH, respectively. As shown in Fig. 5D, the $I_t/I_{max}$ of PCU increased faster than that of PCH, especially during the first 10 min. Significant increases in $I_t/I_{max}$ of PCH were observed at 10–30 min, and from 30 min, a similar increase rate of $I_t/I_{max}$ was observed for both samples. Time-resolved SANS profiles of PCU and PCH are shown in Fig. 6A and B, respectively. Because of the increase in aggregate size, the Guinier feature disappeared at ~20 min, as before. The power law exponents ($m$)

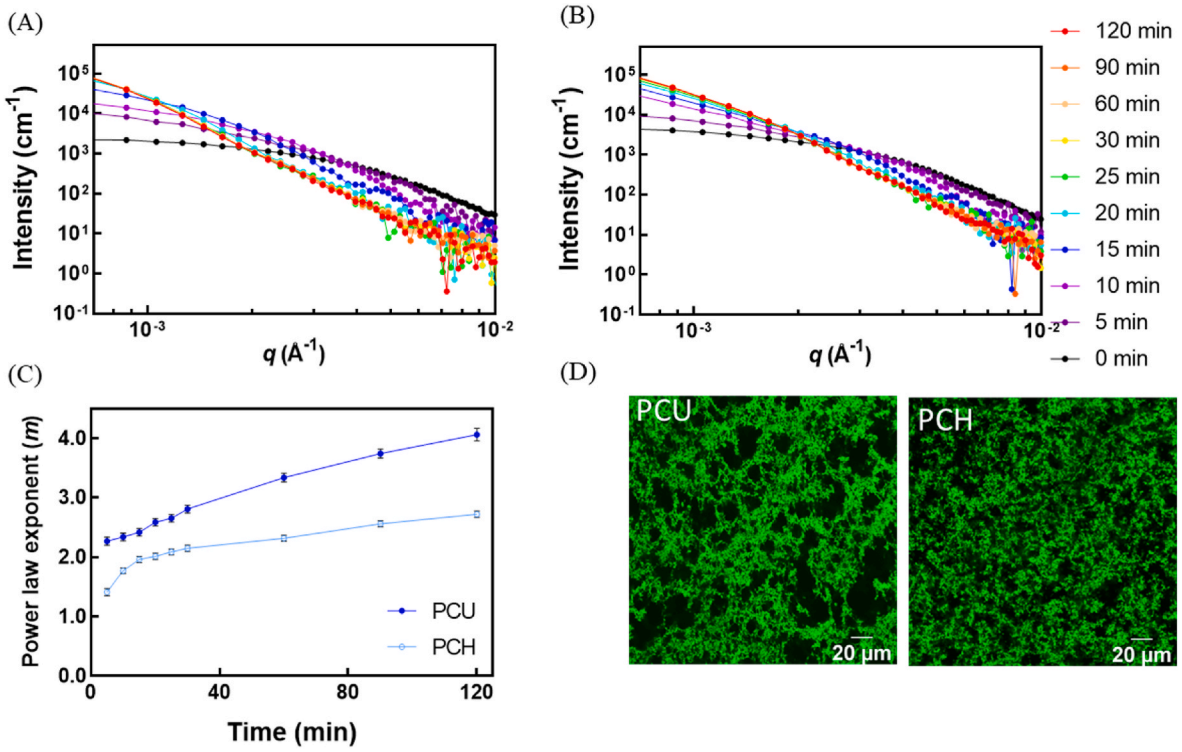


**Fig. 6.** Evolution of time-resolved SANS intensity data at 0.0007 Å$^{-1}$ < $q$ < 0.01 Å$^{-1}$ of (A) PCU and (B) PCH. (C) Power law exponent ($m$) obtained from the power law fitting of SANS results associated with (A) and (B). (D) Confocal laser scanning micro-graphs of PCU and PCH at 2 h. The stained protein networks are in green. The scale bars are 20 μm for both micro-graphs.

obtained from the power law model fits at a low-$q$ range (0.0007 $Å^{-1}$ < $q$ < 0.0022 $Å^{-1}$) are listed in Table S1 and shown in Fig. 6C. Higher power law exponents ($m$) were observed in PCU during the entire reaction and reached ~4 at 120 min. The lower power law exponents ($m$ < 3) of PCH indicated a looser, mass fractal–like structure of the aggregates (Yu et al., 2019). According to the CLSM images at 2 h (Fig. 6D), the observed particles of protein of PCH were smaller than those of PCU. As the firming rate of PCH was slower than of PCU, the presence of small particles may have arisen from the slower rate of aggregation of the proteins. In addition, the faster coagulation rate in PCU may also have resulted in an extensive rearrangement (Mellema, Walstra, van Opheusden, & van Vliet, 2002) through a relatively stronger cross-link but larger voids and a rough aggregate surface [the power law exponent ($m$) was ~4 at 2 h]. Although PCU exhibited large pores, the structure of the proteins showed more interconnectivity than PCH, which could be due to more extensive protein rearrangements in PCU (Yang, Ye, et al., 2023).

According to Yang et al. (2022b), denatured whey proteins that associate with κ-casein on the micellar surface may impair the hydrolysis of κ-casein by pepsin. With a slower hydrolysis rate of κ-casein, heated milk showed a longer coagulation time (Fig. 5B). In addition, the para-casein micelles can be partially stabilised by the denatured whey proteins on the micelle surface, leading to a much slower aggregation rate, i.e. longer coagulation time, lower $G'_{120}$, slower increase in $I_t/I_{max}$ and slower increase in the power law exponents. This is also in agreement with reports on chymosin-induced milk coagulation at pH ~ 6.5, where heat treatment delayed the coagulation process (Anema et al., 2007; Dalgleish, 1990; Raynal & Remeuf, 1998; Singh & Waungana, 2001; Vasbinder, Rollema, & de Kruif, 2003).

### 3.5. Coagulation induced by a combination of pepsin and acid

With the addition of GDL (2%) and a low concentration of pepsin (0.24 U/mL), the pH values of the unheated and heated samples both decreased from 6.7 to ~4.3 after a 2-h reaction time (Fig. 7A). $G'$ exhibited a sequential pattern of a lag phase, followed by an increase phase, subsequent decrease (or flattening) and again an increase at a later time (Fig. 7B). The first significant increase in $G'$ was at ~25.6 min and pH 5.26 for the unheated milk and ~13 min and pH 5.62 for the heated milk. A decrease in $G'$ at ~37.2 min (pH 5.08) and at ~25.5 min (pH 5.18) were observed for unheated and heated milk, respectively (Fig. 7B). The increases in $G'$ again occurred at ~47.8 min (pH 4.97) and 40.7 min (pH 4.80) for unheated and heated milk, respectively (Table 2). The trends in the rheological properties in the CC samples are consistent with the results for the coagulation induced by a combination of GDL and rennet (Herbert, Riaublanc, Bouchet, Gallant, & Dufour, 1999; Lucey, Tamehana, Singh, & Munro, 2000). Compared with the AC samples, the addition of pepsin in CC samples led to shorter coagulation times and higher coagulation pH (Table 2), which was probably due to an accelerated PC at pH > 6 (Lucey et al., 2000). Decreasing the pH of milk has been shown to increase the rate of the hydrolysis (hydrolysis of κ-casein by pepsin), with a maximum at pH 6.0 (Yang et al., 2022a). Aggregation can then occur at a lower extent of κ-casein hydrolysis (van Hooydonk, 1987; Yang et al., 2022a). Thus, compared with the PC sample, the decreasing pH in CC samples could lead to the aggregation of micelles at a lower extent of the hydrolysis of κ-casein and at a shorter coagulation time (van Hooydonk, 1987). At pH < 6 and close to the pI of whey proteins, the associated denatured whey proteins may facilitate such aggregation. A shorter coagulation time and higher $G'$ were found in CCH. The first decrease/flattening in the $G'$ of CC could be due to the excessive large-scale rearrangement of bonds and strands in the protein network (Lucey et al., 2000). At pH < 6, there was partial loosening of bonds within the casein particles in CC due to the solubilisation of CCP (Fig. 2). This solubilisation may alter the balance between viscous and elastic components in the network, may modify protein–protein interactions and may be responsible for the decreases in $G'$ (Lucey et al., 2000). With a further decrease in pH, $G'$ increased again as a result of the transition from a curd exhibiting a pepsin-induced character to a curd exhibiting an acid-induced character (van Vliet, Lakemond, & Visschers, 2004). Reduced electrostatic repulsion at lower pH leads to an increase in hydrophobic interactions (Horne, 1999). Over time, the decrease in $G'$ of CCU at ~110 min could be due to the syneresis of the curd brought about by protein rearrangement (Mellema et al., 2002). In addition, when pH decreased to ~4, the general hydrolysis activity of pepsin

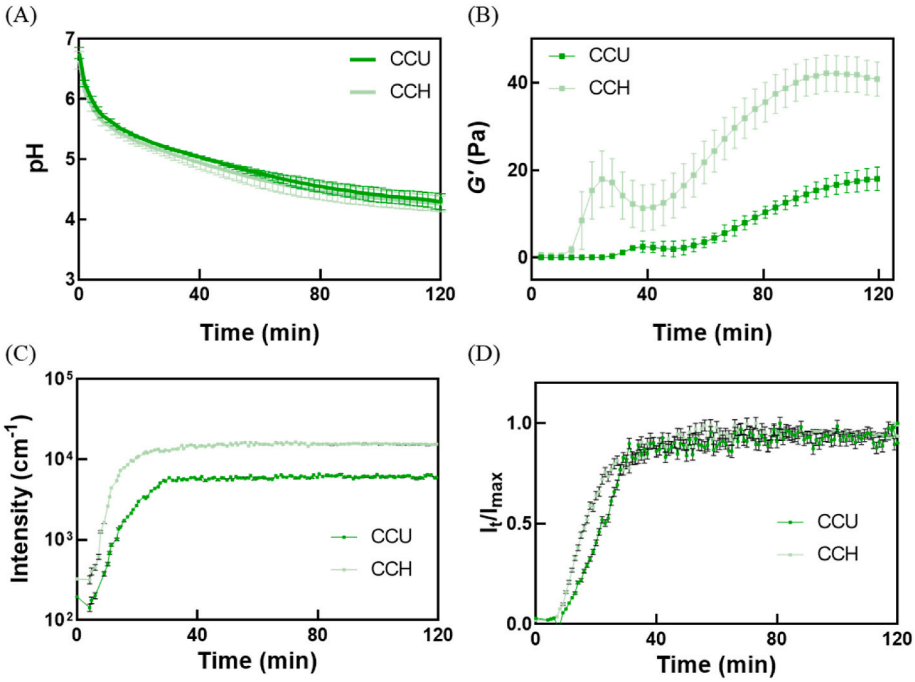


**Fig. 7.** Evolution of pH (A), $G'$ (B), absolute USANS intensity at $q = 1 \times 10^{-4}$ $Å^{-1}$ (C), normalised USANS intensities ($I_t/I_{max}$) (D) for unheated milk (CCU) and heated milk (CCH).

increased (Tam & Whitaker, 1972; Ye, 2021), which decreased $G'$.

The evolution of absolute intensity shows 'first order' characteristics (Fig. 7C). Higher absolute intensity values were observed in CCH compared with CCU. The $I_t/I_{max}$ of CCU and CCH both reached a plateau at ~30 min, with greater rates of increase [higher $d(I_t/I_{max})/dt$] observed for CCH in the first 30 min (Fig. 7D). In agreement with the rheological data, the greater increase in $I_t/I_{max}$ for CCH during the first 30 min could be related to the denatured whey proteins, which accelerate the coagulation rate when the pH decreases.

SANS data (Fig. 8A and **B**) and associated power law model fits of the time-resolved SANS results for CCU and CCH at low $q$ ($0.0007\ Å^{-1} < q < 0.0022\ Å^{-1}$) are listed in Table S1 and shown in Fig. 8C. A slightly lower rate of increase for $m$ was observed in CCU at the first 10 min, whereas a higher $m$ was found from 20 min $m$ reached ~3 for CCH and ~4 for CCU at 30 min. This indicates that a more compact structure was formed in CCH during the first 10 min, but it was not found in CCU until after 20 min. In addition, CCH had a rougher aggregate surface than CCU from 30 min onwards. At 2 h, the micro-structure of CCU was coarse with voids more than 20 μm (Fig. 8D) and the structure of CCH appeared more homogeneous, with smaller voids, mostly ~5 μm (Fig. 8D). These differences could be related to the denatured whey protein incorporated into the curd network.

### 3.6. Samples added with GDL and 2000 U/mL pepsin

With the addition of 2% GDL and 2000 U/mL pepsin, the pH changes were similar to those of the AC and CC samples in the first 2 h and then decreased to ~3.8 after 8 h (Fig. 9A). Coagulation occurred immediately by visual observation after the addition of GDL and a high concentration of pepsin (2000 U/mL). $G'$ increased immediately once the rheological measurements commenced (it took 2 min from the moment when the sample was mixed until the first time point was recorded by the rheometer) and decreased after reaching ~37.8 Pa for unheated milk and ~20.9 Pa for heated milk (Fig. 9B). $G'$ reached a low value after ~80 min for HPU with a decreasing rate of $G'$ ~1.44 Pa/min, whereas $G'$ reached a low value after ~38 min for HPH with a decreasing rate of $G'$ ~3.14 Pa/min (Table 2). The increases in the absolute intensity occurred at the beginning and reached a maximum value within 20 min (Fig. 9C). A decrease in absolute intensity was observed at ~18 and ~41 min for HPH and HPU, respectively. The absolute intensity of the heated sample reached a plateau value (~3000 $cm^{-1}$) after ~1 h, whereas that of the unheated sample reached plateau value after ~4 h (Fig. 9C). The decreases in the intensity agreed with a previous study (Bayrak et al., 2023), which is consistent with the digestion of the milk curd by pepsin. The rate of curd network disruption can be inferred from the decrease in the rate of $I_t/I_{max}$ (Fig. 9D).

As the coagulation proceeded, a progressive increase in the scattering intensity could be observed at $q < 0.003\ Å^{-1}$ in HPU (Fig. 10A), which indicates the formation and growth of large-scale aggregates in the first 10 min. At 15 min (red curve), a decrease in the scattering intensity was found for HPU. As the reaction progressed, a large decrease in the scattering intensity was found for HPH (the absolute intensity of HPH was lower than that of HPU at each time point) (Fig. 10B). The significant decreases in intensity are more related to the general hydrolysis of proteins by pepsin (Bayrak et al., 2023), although the possibility of (micro) phase separation and sedimentation cannot be excluded (Fig. S2). As shown in Fig. 10C, an increase in the power law exponent ($m$) was found in the first 10 min for both samples. $m$ reached a maximum value at 15 min for HPU (~3.2) and HPH (~4.0). Over time, $m$ for HPU was ~3.1 from 20 min to 8 h, whereas a reduction of $m$ was found for HPH, suggesting the loosening of the aggregate micro-structure as digestion proceeded.

The decrease in pH in the presence of 2000 U/g pepsin in the HP sample simulates the gastric digestion environment where milk is ingested. For the first 5 min, the pH of the samples was >6, which was greater than the pI of casein proteins. At this pH (>6), coagulation occurred because of the pepsin-induced specific hydrolysis of κ-casein (Yang et al., 2022a), as shown by the increases in $G'$ (Fig. 9B) and

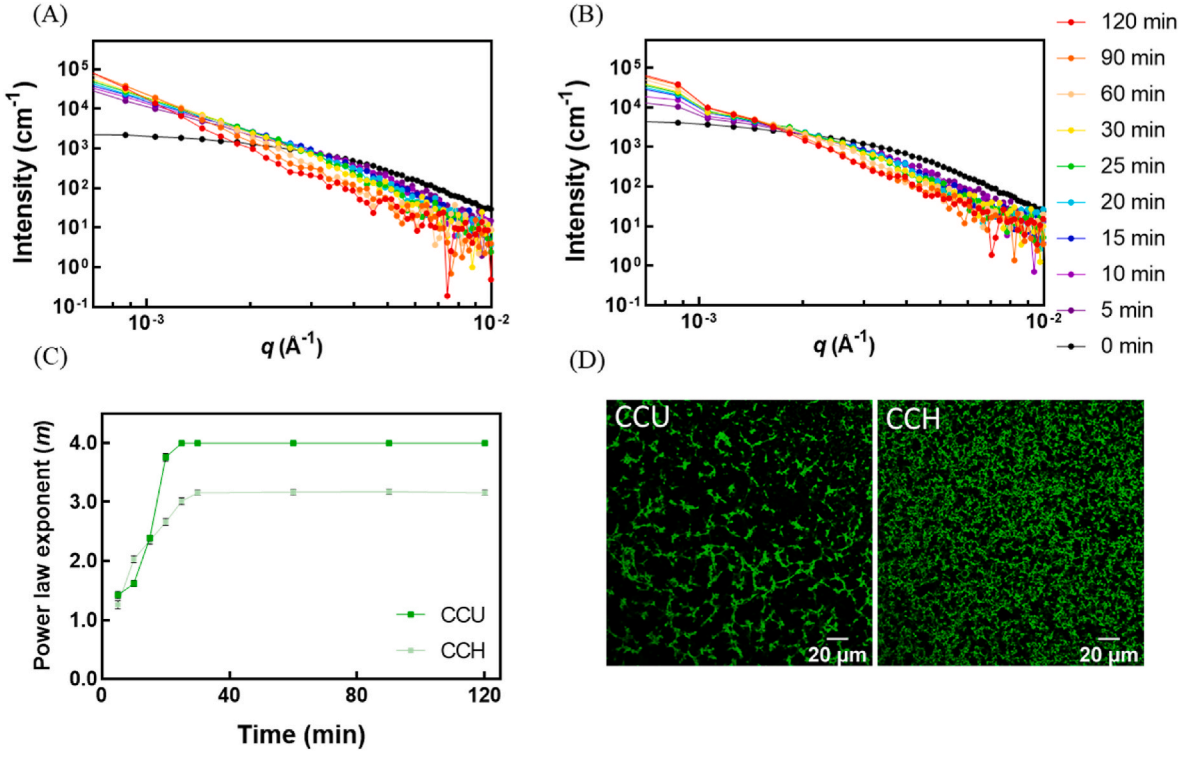


**Fig. 8.** Evolution of time-resolved SANS intensity data at $0.0007\ Å^{-1} < q < 0.01\ Å^{-1}$ of (A) CCU and (B) CCH. (C) Power law exponent ($m$) obtained from the power law fitting of SANS associated with (A) and (B). (D) Confocal laser scanning micro-graphs of CCU and CCH at 2 h. The stained protein networks are in green. The scale bars are 20 μm for both micro-graphs.

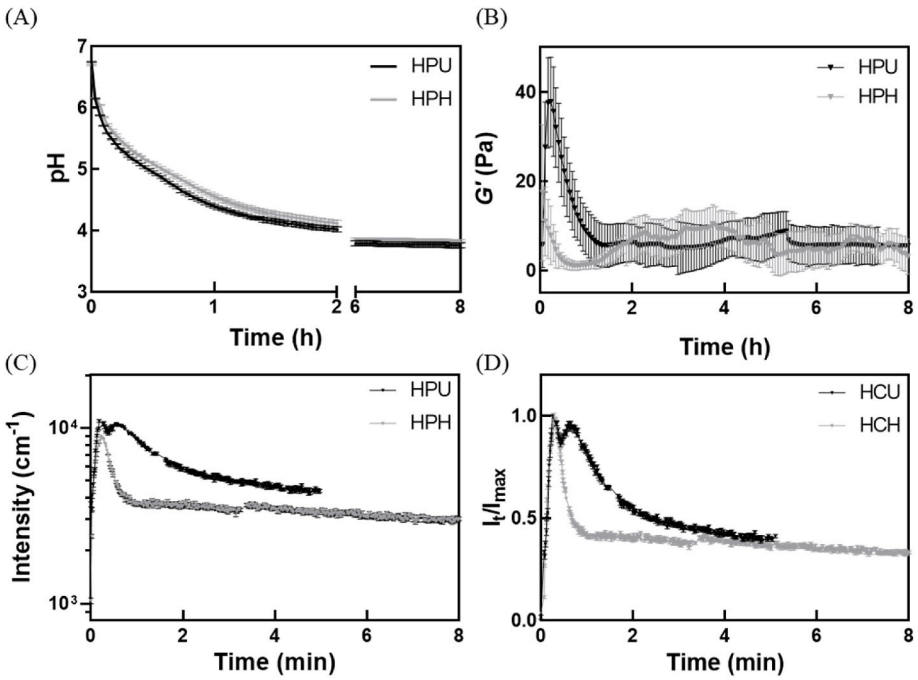


**Fig. 9.** Evolution of pH (A), $G'$ (B), absolute USANS intensity at $q = 1 \times 10^{-4}$ Å$^{-1}$ (C), normalised USANS intensities ($I_t/I_{max}$) (D) for unheated milk (HPU) and heated milk (HPH).

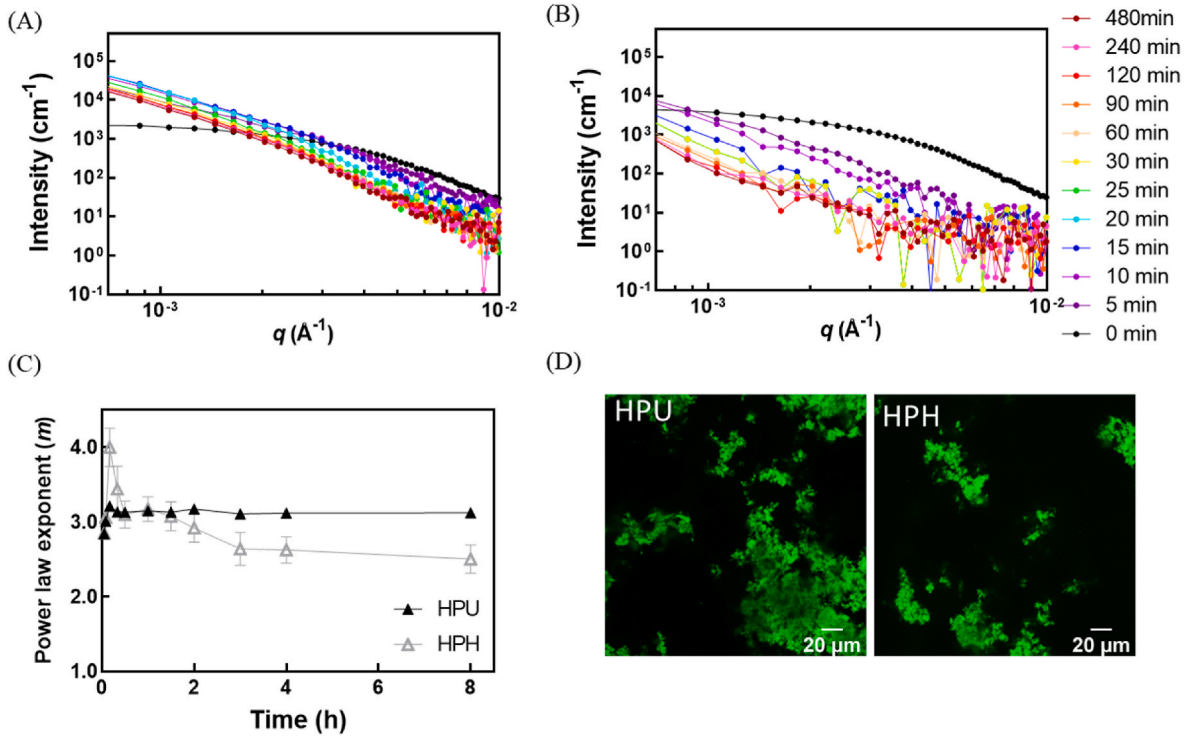


**Fig. 10.** Evolution of time-resolved SANS intensity data at 0.0007 Å$^{-1}$ < $q$ < 0.01 Å$^{-1}$ of (A) HPU and (B) HPH. (C) Power law exponent ($m$) obtained from the power law fitting of SANS results associated with (A) and (B). (D) Confocal laser scanning micro-graphs of HPU and HPH at 8 h. The stained protein networks are in green. The scale bars are 20 μm for both micro-graphs.

absolute intensity (Fig. 9C), and the activity of pepsin for general hydrolysis was relatively low (Kageyama, 2002). In addition, at pH > 6, the associated denatured whey proteins performed a barrier role in the network of heated-milk proteins (Yang, Ye, et al., 2023). Over time, pH gradually decreased and the general hydrolysis activity of pepsin increased. The curd structure was gradually broken down as most of the proteins were hydrolysed. Decreases in $G'$ (Fig. 9B) and absolute intensity (Fig. 9C) were observed for both HPU and HPH. In addition, decreases in the low-$q$ power law exponent ($m$) were observed for both samples (Fig. 10C), suggesting that the aggregated micelles in the protein curd network (on a ~100 nm scale) were degraded because of the hydrolysis of the curd into smaller protein fragments, peptides or amino

acids, which is in agreement with the results from the study by (Bayrak et al., 2023). Compared with HPU, the relatively faster decrease in firmness (Fig. 9B) and $I_t/I_{max}$ (Fig. 9D) of HPH indicates a faster rate of curd degradation (due to the general hydrolysis of proteins by pepsin) of HPH. These might be attributed to the higher ease of diffusion of pepsin in the looser curd structure of HPH than that of HPU. Over time, the pH gradually decreased further to <5 and the hydrolytic activity of pepsin increased. This is in agreement with the effect of heat treatment on the digestibility of milk proteins in a simulated gastric environment (Ye et al., 2017). The micro-structures of HPU and HPH after 8 h of incubation observed by CLSM are shown in Fig. 10D, where a large pore area (serum) can be observed in both HPU and HPH. Photographs of HPU and HPH are shown in Fig. S2, which demonstrate low turbidity (transparency); HPU and HPH are transparent, while the other samples are white. As the reaction progressed, the curd was gradually broken down as most of the proteins were hydrolysed by pepsin.

Coagulation time can be estimated from the rheological results. Information on the level of structural complexity or fractal-like nature of milk aggregates can be obtained from a SANS power law exponent and should be complemented by CLSM micro-graphs. At $q = 1 \times 10^{-4}$ Å$^{-1}$, the change in absolute intensity is positively related to the change in $G'$ when plotted as a function of time (Fig. 3B and **C**). In agreement with previous studies (Bayrak et al., 2023; Huang, Terech, Raghavan, & Weiss, 2005), plotting scattering intensities at a single $q$ value as a function of time is an efficient method for assessing the aggregation kinetics of protein network samples. Although finite times are required for sufficient increases in $G'$ to be identified by rheometry, the changes in the absolute intensity at this fixed $q$ value in USANS could be observed from the beginning, which is in agreement with the study by Yang, Cheng, et al. (2023). This study highlights the importance of using complementary measurement techniques, including USANS and SANS, that are sensitive to multiple length scales.

According to the SANS results, regardless of coagulation, the surface roughness of the aggregates in the heated milk was greater than that in the unheated samples. However, heat treatment has different effects on aggregate formation in acid-induced, pepsin-induced and milk gels induced by a combination of pepsin and acid. Heat treatment facilitated acid-induced coagulation but retarded the pepsin-induced coagulation. In general, pH plays a crucial role in milk coagulation and significantly affects the impact of heat treatment on this process. When milk is sufficiently preheated, denatured whey proteins associate with casein micelles and the impact on the gel network varies with pH conditions. At pH > 6, which is higher than the pI of whey proteins, the associated whey proteins act as a barrier layer between casein micelles against coagulation. However, closer to the pI, the associated whey proteins initiate isoelectric precipitation/aggregation. According to Yang, Ye, et al. (2023), pepsin-induced heated-milk coagulation is retarded at pH 6.3 but is enhanced at pH 6.0. With a continuous decrease in pH (by addition of GDL), regardless of the presence of pepsin, heated-milk coagulation takes place at higher pH (between pH 5.0 and 6.0) than that for unheated milk and higher $G'$. This could be due to the increased cross-linking or bridging by denatured whey proteins within gels made from heated milk (Lucey et al., 1997). During the simulated *in vitro* gastric digestion process, pepsin-induced coagulation occurred at pH > 6 (Yang et al., 2022a). At this pH, the associated whey proteins produced a barrier effect for para-casein micelle coagulation, resulting in looser protein curd. As the pH decreased to <4, the disintegration and hydrolysis of proteins by pepsin occurred more rapidly in the softer curd formed in the heated milk.

## 4. Conclusions

The nature of milk coagulation affects the diverse structural properties of the milk curd. Rheological measurements have enabled the differentiation of the properties of curd produced by the action of acid, pepsin or a combination of acid and pepsin. Using USANS, SANS and CLSM methods, it has been possible to demonstrate that milk curd with distinct rheological properties exhibits different structures at multi-scale levels. The size and volume fraction of the aggregates increase over time during the process of aggregation. Heat treatment leads to the association of denatured whey proteins with κ-casein on the surface of casein micelles, which has different effects on the curd induced by acid, pepsin and their combination. In the presence of a high pepsin concentration, faster coagulation and degradation of milk curd were observed in heated-milk samples. This study provides further understanding of the effect of heat treatment on milk coagulation and the curd degradation process.

## CRediT authorship contribution statement

**Mengxiao Yang:** Writing – original draft, Methodology, Investigation, Formal analysis, Data curation, Conceptualization. **Aiqian Ye:** Writing – review & editing, Supervision, Resources, Project administration, Funding acquisition, Conceptualization. **Zhi Yang:** Writing – review & editing, Supervision. **David W. Everett:** Writing – review & editing, Supervision. **Liliana de Campo:** Investigation, Data curation. **Harjinder Singh:** Writing – review & editing, Supervision. **Elliot Paul Gilbert:** Writing – review & editing, Supervision, Methodology, Investigation, Conceptualization.

## Declaration of competing interest

There are no conflicts of interest to declare.

## Data availability

Data will be made available on request.

## Acknowledgments

This work was supported by the New Zealand Ministry of Business, Innovation and Employment (Wellington, New Zealand), via the programme “New Zealand Milks Mean More” (MAUX1803), and the Tertiary Education Commission, via the Riddet Institute–New Zealand Centre of Research Excellence. The author Mengxiao Yang thanks the Australian Institute of Nuclear Science and Engineering (AINSE) for a Post Graduate Research Award. The authors acknowledge the support of the Australian Centre for Neutron Scattering, ANSTO, and theAustralian Government through the National Collaborative Research Infrastructure Strategy in supporting the QUOKKA and KOOKABURRA neutron research infrastructure used in this work via ACNS proposal P9635 and previous BILBY data via proposal P8703.

## Appendix A. Supplementary data

Supplementary data to this article can be found online at https://doi.org/10.1016/j.foodhyd.2024.110681.

## References

Anema, S. G., Lee, S. K., & Klostermeyer, H. (2007). Effect of pH at heat treatment on the hydrolysis of κ-casein and the gelation of skim milk by chymosin. *LWT-Food Science & Technology, 40*(1), 99–106.

Anema, S. G., Lee, S. K., & Klostermeyer, H. (2011). Rennet-induced aggregation of heated pH-adjusted skim milk. *Journal of Agricultural and Food Chemistry, 59*(15), 8413–8422.

Bayrak, M., Mata, J., Raynes, J. K., Greaves, M., White, J., Conn, C. E., … Logan, A. (2021). Investigating casein gel structure during gastric digestion using ultra-small and small-angle neutron scattering. *Journal of Colloid and Interface Science, 594*, 561–574.

Bayrak, M., Whitten, A. E., Mata, J., Conn, C. E., Floury, J., & Logan, A. (2023). Real-time monitoring of casein gel microstructure during simulated gastric digestion monitored by small-angle neutron scattering. *Food Hydrocolloids, 108919*.

Brodkorb, A., Egger, L., Alminger, M., Alvito, P., Assunção, R., Ballance, S., … Carrière, F. (2019). INFOGEST static in vitro simulation of gastrointestinal food digestion. *Nature Protocols, 14*(4), 991–1014.

Callaghan-Patrachar, N., Peyronel, F., Pink, D., Marangoni, A., & Adams, C. (2021). USANS and SANS investigations on the coagulation of commercial bovine milk: Microstructures induced by calf and fungal rennet. *Food Hydrocolloids, 116*, Article 106622.

Chodankar, S., Aswal, V. K., Kohlbrecher, J., Vavrin, R., & Wagh, A. G. (2009). Small-angle neutron scattering study of structure and kinetics of temperature-induced protein gelation. *Physical Review E, 79*(2), Article 021912. https://doi.org/10.1103/PhysRevE.79.021912

Dalgleish, D. G. (1990). Denaturation and aggregation of serum proteins and caseins in heated milk. *Journal of Agricultural and Food Chemistry, 38*(11), 1995–1999.

Dalgleish, D. G., Brinkhuis, J., & Payens, T. A. (1981). The coagulation of differently sized casein micelles by rennet. *European Journal of Biochemistry, 119*(2), 257–261.

Day, L., Raynes, J., Leis, A., Liu, L., & Williams, R. (2017). Probing the internal and external micelle structures of differently sized casein micelles from individual cows milk by dynamic light and small-angle X-ray scattering. *Food Hydrocolloids, 69*, 150–163.

de Kruif, C. G. (2014). The structure of casein micelles: A review of small-angle scattering data. *Journal of Applied Crystallography, 47*(5), 1479–1489.

De Wit, J. (1981). Structure and functional behaviour of whey proteins. *Netherlands Milk and Dairy Journal, 35*, 47–64.

Gilbert, E. P. (2019). Small-angle X-Ray and neutron scattering in food colloids. *Current Opinion in Colloid & Interface Science, 42*, 55–72.

Gilbert, E. P. (2023). Neutron techniques for food hydrocolloids. *Current Opinion in Colloid & Interface Science*, Article 101730.

Hammouda, B. (2010). A new Guinier–Porod model. *Journal of Applied Crystallography, 43*(4), 716–719.

Herbert, S., Riaublanc, A., Bouchet, B., Gallant, D., & Dufour, E. (1999). Fluorescence spectroscopy investigation of acid-or rennet-induced coagulation of milk. *Journal of Dairy Science, 82*(10), 2056–2062.

Horne, D. S. (1999). Formation and structure of acidified milk gels. *International Dairy Journal, 9*(3–6), 261–268.

Horne, D., & Lucey, J. (2014). Revisiting the temperature dependence of the coagulation of renneted bovine casein micelles. *Food Hydrocolloids, 42*, 75–80.

Huang, X., Terech, P., Raghavan, S. R., & Weiss, R. G. (2005). Kinetics of 5α-cholestan-3β-yl N-(2-naphthyl) carbamate/n-alkane organogel formation and its influence on the fibrillar networks. *Journal of the American Chemical Society, 127*(12), 4336–4344.

Huppertz, T., & Chia, L. W. (2021). Milk protein coagulation under gastric conditions: A review. *International Dairy Journal*, Article 104882.

Kageyama, T. (2002). Pepsinogens, progastricsins, and prochymosins: Structure, function, evolution, and development. *Cellular and Molecular Life Sciences CMLS, 59*, 288–306.

Kline, S. R. (2006). Reduction and analysis of SANS and USANS data using IGOR Pro. *Journal of Applied Crystallography, 39*(6), 895–900.

Lewis, M. (1994). Heat treatment of milk. In *Robinson: Modern dairy Technology* (pp. 1–60). Springer.

Li, Z., Yang, Z., Otter, D., Rehm, C., Li, N., Zhou, P., et al. (2018). Rheological and structural properties of coagulated milks reconstituted in D2O: Comparison between rennet and a tamarillo enzyme (tamarillin). *Food Hydrocolloids, 79*, 170–178.

Liu, D., Yu, Y., Zhang, J., Liu, X., Wang, M., Hemar, Y., … Zhou, P. (2017). Biochemical and physico-chemical changes of skim milk during acidification with glucono-δ-lactone and hydrogen chloride. *Food Hydrocolloids, 66*, 99–109.

Lucey, J. A. (2017). Formation, structural properties, and rheology of acid-coagulated milk gels. In *Cheese* (pp. 179–197). Elsevier.

Lucey, J., Tamehana, M., Singh, H., & Munro, P. (1998). A comparison of the formation, rheological properties and microstructure of acid skim milk gels made with a bacterial culture or glucono-δ-lactone. *Food Research International, 31*(2), 147–155.

Lucey, J. A., Tamehana, M., Singh, H., & Munro, P. A. (2000). Rheological properties of milk gels formed by a combination of rennet and glucono-δ-lactone. *Journal of Dairy Research, 67*(3), 415–427.

Lucey, J. A., Tamehana, M., Singh, H., & Munro, P. A. (2001). Effect of heat treatment on the physical properties of milk gels made with both rennet and acid. *International Dairy Journal, 11*(4–7), 559–565.

Lucey, J. A., Teo, C. T., Munro, P. A., & Singh, H. (1997). Rheological properties at small (dynamic) and large (yield) deformations of acid gels made from heated milk. *Journal of Dairy Research, 64*(4), 591–600.

Lucey, J. A., Wilbanks, D. J., & Horne, D. S. (2022). Impact of heat treatment of milk on acid gelation. *International Dairy Journal, 125*, Article 105222.

Martin, J. E., & Hurd, A. (1987). Scattering from fractals. *Journal of Applied Crystallography, 20*(2), 61–78.

Mata, J. P., Udabage, P., & Gilbert, E. P. (2011). Structure of casein micelles in milk protein concentrate powders via small angle X-ray scattering. *Soft Matter, 7*(8), 3837–3843.

Mellema, M., Walstra, P., van Opheusden, J. H. J., & van Vliet, T. (2002). Effects of structural rearrangements on the rheology of rennet-induced casein particle gels. *Advances in Colloid and Interface Science, 98*(1), 25–50.

Miranda, G., & Pelissier, J. P. (1983). Kinetic studies of in vivo digestion of bovine unheated skim-milk proteins in the rat stomach. *Journal of Dairy Research, 50*(1), 27–36.

Moitzi, C., Menzel, A., Schurtenberger, P., & Stradner, A. (2011). The pH induced sol–gel transition in skim milk revisited. A detailed study using time-resolved light and X-ray scattering experiments. *Langmuir, 27*(6), 2195–2203.

Oldfield, D. J., Singh, H., Taylor, M. W., & Pearce, K. N. (2000). Heat-induced interactions of β-lactoglobulin and α-lactalbumin with the casein micelle in pH-adjusted skim milk. *International Dairy Journal, 10*(8), 509–518.

Pasquier, J., Brûlet, A., Boire, A., Jamme, F., Perez, J., Bizien, T., … Boué, F. (2019). Monitoring food structure during digestion using small-angle scattering and imaging techniques. *Colloids and Surfaces A: Physicochemical and Engineering Aspects, 570*, 96–106.

Plowman, J. E., & Creamer, L. K. (1995). Restrained molecular dynamics study of the interaction between bovine κ-casein peptide 98–111 and bovine chymosin and porcine pepsin. *Journal of Dairy Research, 62*(3), 451–467.

Raynal, K., & Remeuf, F. (1998). The effect of heating on physicochemical and renneting properties of milk: A comparison between caprine, ovine and bovine milk. *International Dairy Journal, 8*(8), 695–706.

Rehm, C., Brûlé, A., Freund, A. K., & Kennedy, S. J. (2013). Kookaburra: The ultra-small-angle neutron scattering instrument at OPAL. *Journal of Applied Crystallography, 46*(6), 1699–1704.

Rehm, C., Campo, L.d., Brûlé, A., Darmann, F., Bartsch, F., & Berry, A. (2018). Design and performance of the variable-wavelength Bonse–Hart ultra-small-angle neutron scattering diffractometer KOOKABURRA at ANSTO. *Journal of Applied Crystallography, 51*(1), 1–8.

Roy, D., Ye, A., Moughan, P. J., & Singh, H. (2020). Gelation of milks of different species (dairy cattle, goat, sheep, red deer, and water buffalo) using glucono-δ-lactone and pepsin. *Journal of Dairy Science, 103*(7), 5844–5862.

Schaefer, D. W., Martin, J. E., Wiltzius, P., & Cannell, D. S. (1984). Fractal geometry of colloidal aggregates. *Physical Review Letters, 52*(26), 2371.

Singh, H. (1995). Heat-induced changes in casein, including interactions with whey proteins. *Bulletin-International Dairy Federation*, (1), 86–104.

Singh, R., Hemar, Y., Gilbert, E. P., Wu, Z., & Yang, Z. (2020). Effect of genipin cross-linking on the structural features of skim milk in the presence of ethylenediaminetetraacetic acid (EDTA). *Colloids and Surfaces A: Physicochemical and Engineering Aspects, 603*, Article 125174.

Singh, H., & Waungana, A. (2001). Influence of heat treatment of milk on cheesemaking properties. *International Dairy Journal, 11*(4–7), 543–551.

Sokolova, A., Whitten, A. E., de Campo, L., Christoforidis, J., Eltobaji, A., Barnes, J., … Berry, A. (2019). Performance and characteristics of the BILBY time-of-flight small-angle neutron scattering instrument. *Journal of Applied Crystallography, 52*(1), 1–12.

Tam, J. J., & Whitaker, J. R. (1972). Rates and extents of hydrolysis of several caseins by pepsin, rennin, Endothia parasitica protease and Mucor pusillus protease. *Journal of Dairy Science, 55*(11), 1523–1531.

van Hooydonk, A. M. (1987). *The renneting of milk: A kinetic study of the enzymic and aggregation reactions*. Wageningen University and Research.

van Vliet, T., Lakemond, C. M., & Visschers, R. W. (2004). Rheology and structure of milk protein gels. *Current Opinion in Colloid & Interface Science, 9*(5), 298–304.

Vasbinder, A., Rollema, H., & de Kruif, C. (2003). Impaired rennetability of heated milk; study of enzymatic hydrolysis and gelation kinetics. *Journal of Dairy Science, 86*(5), 1548–1555.

Wang, Y., Eastwood, B., Yang, Z., de Campo, L., Knott, R., Prosser, C., … Hemar, Y. (2019). Rheological and structural characterization of acidified skim milks and infant formulae made from cow and goat milk. *Food Hydrocolloids, 96*, 161–170.

Wood, K., Mata, J. P., Garvey, C. J., Wu, C.-M., Hamilton, W. A., Abbeywick, P., … Booth, N. (2018). QUOKKA, the pinhole small-angle neutron scattering instrument at the OPAL research reactor, Australia: Design, performance, operation and scientific highlights. *Journal of Applied Crystallography, 51*(2), 294–314.

Yang, Z., Cheng, L., de Campo, L., Gilbert, E. P., Mittelbach, R., Luo, L., … Hemar, Y. (2023). Microstructural evolution during acid induced gelation of cow, goat, and sheep milk probed by time-resolved (ultra)-small angle neutron scattering. *Food Hydrocolloids, 137*, Article 108381.

Yang, Z., de Campo, L., Gilbert, E. P., Knott, R., Cheng, L., Storer, B., … Hemar, Y. (2022c). Effect of NaCl and CaCl2 concentration on the rheological and structural characteristics of thermally-induced quinoa protein gels. *Food Hydrocolloids, 124*, Article 107350.

Yang, M., Ye, A., Yang, Z., Everett, D. W., Gilbert, E. P., & Singh, H. (2022a). Kinetics of pepsin-induced hydrolysis and the coagulation of milk proteins. *Journal of Dairy Science, 105*(2), 990–1003.

Yang, M., Ye, A., Yang, Z., Everett, D. W., Gilbert, E. P., & Singh, H. (2022b). Pepsin-induced coagulation of casein micelles: Effect of whey proteins and heat treatment. *Food Chemistry, 134214*.

Yang, M., Ye, A., Yang, Z., Everett, D. W., Gilbert, E. P., & Singh, H. (2023). Pepsin-induced coagulation of casein micelles: Effect of whey proteins and heat treatment. *Food Chemistry, 402*, Article 134214.

Ye, A. (2021). Gastric colloidal behaviour of milk protein as a tool for manipulating nutrient digestion in dairy products and protein emulsions. *Food Hydrocolloids, 106599*.

Ye, A., Cui, J., Dalgleish, D., & Singh, H. (2017). Effect of homogenization and heat treatment on the behavior of protein and fat globules during gastric digestion of milk. *Journal of Dairy Science, 100*(1), 36–47.

Ye, A., Liu, W., Cui, J., Kong, X., Roy, D., Kong, Y., … Singh, H. (2019). Coagulation behaviour of milk under gastric digestion: Effect of pasteurization and ultra-high temperature treatment. *Food Chemistry, 286*, 216–225.

Yu, L., Yakubov, G. E., Gilbert, E. P., Sewell, K., van de Meene, A. M., & Stokes, J. R. (2019). Multi-scale assembly of hydrogels formed by highly branched arabinoxylans from Plantago ovata seed mucilage studied by USANS/SANS and rheology. *Carbohydrate Polymers, 207*, 333–342.

Zhu, H., & Damodaran, S. (1994). Heat-induced conformational changes in whey protein isolate and its relation to foaming properties. *Journal of Agricultural and Food Chemistry, 42*(4), 846–855.